A REGULARIZED INTERFACE MODEL FOR SIMULATING THE RESPONSE OF ADHESIVE JOINTS

N. Valoroso*

"Parthenope" University of Naples, Department of Engineering, Italy
Centro Direzionale Isola C4, 80143 – Napoli, Tel. +39 081 5476720
*Corresponding author's e-mail address: nunziante.valoroso@uniparthenope.it

ABSTRACT

A regularized interface damage model is presented grounded on the cohesive-zone concept. This is obtained using a gradient-based formulation, which is equivalent to the introduction of the laplacian of a scalar damage field into the threshold function of the corresponding local model. Unlike the classical cohesive-zone formulations, damage is driven by a non-local energy release rate and the size of the process zone is controlled by an independent model parameter. The capabilities of the proposed approach are show via a mode-I fracture problem for an adhesive joint. Numerical results illustrate the effects of the gradient dependence against the usual cohesive zone implementation.

KEYWORDS: Adhesive joints, fracture, interface, cohesive-zone models, damage, regularization, gradient

1. INTRODUCTION

Adhesive bonding offers improved performances in a number of industrial applications with respect to mechanical fastening methods. Actually, adhesives provide electrical insulation, are able to seal and to bridge tolerances, do not require heat input as welding does and transmit stresses in a more uniform way compared to bolts and rivets. When employing adhesive bonding in structures, designers are generally interested in the possibility of determining the strain and stress state in the joint and the sensitivity of the bond strength to unavoidable imperfections. To this end, a variety of approaches can be used, ranging from linear elastic considerations based on a fully analytical approach up to sophisticated elasto-plastic, visco-elastic, fracture or damage models and related numerical methods [1].

Typically, the adhesive stratum is the weakest link in a structural joint and the bond region has a thickness that is small compared to the size of the adherends and to its in-plane dimensions. Therefore, adhesive layers can be conveniently schematized as interfaces where all nonlinearities are lumped. In such cases, displacement discontinuities are allowed across the joined surfaces and the relevant tractions depend from such jumps in the displacement field via a constitutive relationship that is independent from the one of the bulk material. In particular, the interface constitution can be specified either in the form of a damage model or by directly prescribing the softening curve. Both of them provide an equivalent, macroscopic description for the de-cohesion process of atomic lattices [11].

The cohesive-zone concept, initially introduced by Barenblatt [3] and first used by Hillerborg et al. [7] in a finite element setting, has become widespread in recent years. The reasons of its success are manifold, among which are the elimination of the stress singularities of Linear Elastic Fracture Mechanics and the key ability of the approach to describe the fracture process starting from the nucleation phase up to complete separation.

Cohesive-zone models are intrinsically phenomenological, whereby they can cover a number of materials and fracture mechanisms by suitably tuning the nonlinear relationship between displacement jumps, which are understood as interface strains, and the surface tractions, playing the role of stresses [2]. In current implementations, cohesive models are used along with interface elements located at sites where the potential crack trajectories can develop and lead to the formation of traction-free surfaces [10].

The present work is motivated by the author's attempt to obtain quantitative predictions for adhesively bonded assemblies that fail with large cohesive regions. For instance, this may occur for epoxy adhesives, see e.g. [9], and it is even more evident when using adhesives modified with the addition of rubber-like nanoparticles [14], which exhibit high ductility. To this end, the original damage-based formulation originally proposed in [16] is revisited and enriched via a gradient enhancement.

Gradient-based formulations have emerged in the 1990s as regularizing techniques for continuum

Date of submission/acceptance: 31.05.2024/15.12.2024 http://doi.org/10.35219/awet.2024.12

damage models [12]. Actually, in such models, the constitutive equations do include differential or averaging operators that put into effect the necessary regularity of strains or internal variables to restore objectivity, see e.g. [8], [13] and references therein. In classical cohesive models, strain localization is not a major issue since damage behaviour is already restricted to the interface. However, when simulating progressive damage with zero-thickness interface elements, a number of difficulties are still present that are related to the definition of the model parameters (interface stiffness and cohesive strength, above all) and to the mesh design, which should be able to capture the extension of the process zone and the distribution of the cohesive forces within it. In this respect, the proposed gradient enhancement is expected to be useful in smoothing the solution over elements.

The outline of the paper is as follows. Section 2 starts with a summary of the local model equations, which are specialized to the case of the damage function that produces the exponential traction-separation law presented in [16]. The gradient-based model is next developed by considering a free energy functional that includes a quadratic term in the gradient of damage. As shown later on in the paper, one of the effects of introducing the gradient of damage in the formulation is that of expanding the size of the cohesive process zone ahead of the crack tip with respect to the one obtained using the underlying local model. The new interface model is recognized to have several common features with the graded damage model contributed in [19], [20]; among others is the fact that it fits in the generalized standard setting [5], whereby a normality rule holds.

In Section 3, the implementation of the coupled structural problem based upon a staggered solution scheme is outlined first. Numerical results are then presented for a symmetric double cantilever beam structure in mode-I bending. The effects of the gradient-based enhancement are demonstrated by comparing the extension of the process zone, the damage distribution along the interface and the global response curve of the structure against the analogous outcomes of the local model.

Conclusions and future research directions are finally given in Section 4.

2. DAMAGE-BASED COHESIVE MODEL

As a model problem consider the two-dimensional structure in figure 1, consisting of two elastic bodies that are assembled together by a thin adhesive layer that can experience damage upon loading.

For the developments that follow, attention will be restricted to opening mode only, whereby tractions and jumps are normal to the interface, and irreversible behaviour will be introduced by appealing to a damage mechanics-based formulation inspired by [16].

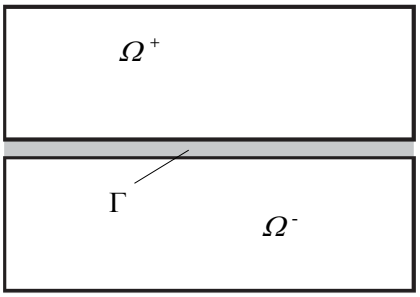

Fig. 1. Adhesive assembly. Model problem

2.1. The Local Model

Let the energy density function for the interface be

$$\psi(s,d) = \frac{1}{2}\omega(d)k^+\langle s\rangle_+^2 + \frac{1}{2}k^-\langle s\rangle_-^2 \qquad (1)$$

where $s = u^+ - u^-$ is the displacement jump, the brackets $\langle\cdot\rangle_+$ and $\langle\cdot\rangle_-$ stand for the positive and negative part of the argument, the $k^\pm$ are the stiffness coefficients (k^- is a penalty stiffness that prevents interpenetration) and ω is a decreasing function of the scalar damage variable d accounting for material degradation. The constitutive equations for the surface traction t and the damage-driving force Y read:

$$t = \frac{\partial\psi}{\partial s} = \omega(d)k^+\langle s\rangle_+ + k^-\langle s\rangle_- \qquad (2)$$

$$Y = -\frac{\partial\psi}{\partial d} = -\frac{1}{2}\omega'(d)k^+\langle s\rangle_+^2 \qquad (3)$$

Damage d is a constrained variable, i.e. $d \in [0,1]$, and its evolution law can be obtained by prescribing a dissipation function in the form

$$\varphi(\dot{d}) = Y_c(d)\dot{d} + H(\dot{d}) \qquad (4)$$

where $\dot{d}$ is the damage time rate, $Y_c(d)$ is the critical force that defines the instantaneous elastic limit and H is a function that ensures irreversibility, that is $\dot{d} \geq 0$. The usual thermodynamic argument provides the normality rule of generalized standard models [5]:

$$f(Y,d) \leq 0; \quad \dot{d} \geq 0; \quad f(Y,d)\,\dot{d} = 0 \qquad (5)$$

where $f(Y,d)$ designates the damage loading function.

Typical forms of $f(Y,d)$ are exponentials, polynomials or rational functions and their expressions can be related to a specific softening curve. For example, the exponential traction-separation curve depicted in figure 2 can be obtained using [16]:

$$f(Y,d) = Y - \omega'(d)\big[(G_c - Y_0)\ln\big(\omega(d)\big) - Y_0\big] \qquad (6)$$

G_c being the fracture energy of the material and Y_0 the elastic energy at damage onset, which in turn depends upon G_c, k^+ and the cohesive strength σ_c.

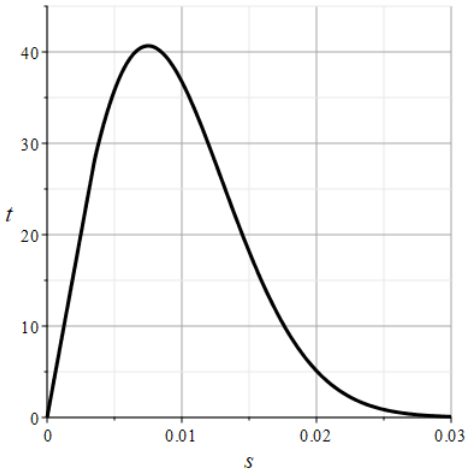

Fig. 2. Exponential traction-separation law

In a local model the material parameters G_c and σ_c do establish the link between the microscopic fracture mechanisms and the phenomenological description; they also induce a length scale [7]:

$$l_H = \frac{E\, G_c}{\sigma_c^2} \tag{7}$$

where E is understood as the elastic modulus of the adherends. Equation (7) provides a rough estimate for the size of the cohesive process zone, see also [6], [18] for alternative expressions; moreover, it can also be interpreted as measure of material brittleness, i.e. the smaller l_H the more brittle the material. Actually, for vanishing l_H compared to the characteristic dimension of the structure, fracture behaviour can be fully captured using Linear Elastic Fracture Mechanics, in which case the process zone collapses to a single point.

2.1 The Gradient Enhancement

The introduction of the spatial gradient of damage into the constitutive equations changes the local equations into a new boundary value problem that is coupled to the usual equilibrium equations. In particular, in this case the dissipation potential is obtained by integrating the function (4) over the interface domain Γ:

$$D(\dot{d}) = \int_\Gamma \varphi(\dot{d})\, \mathrm{d}x \tag{8}$$

whereas the internal energy functional is taken as:

$$\Psi(s,d) = \int_\Gamma \psi(s,d)\mathrm{d}x + \frac{1}{2}\int_\Gamma c\, \|\nabla d\|^2 \mathrm{d}x \tag{9}$$

In the above relationship $c \geq 0$ is a constant with physical dimensions of a force that can be linked to a length parameter characterizing the size of the process zone. The first variation of the internal energy (9) with respect to damage and the divergence theorem give the energy release rate G:

$$G = Y + c\, div(\nabla d) \tag{10}$$

along with the boundary condition:

$$\nabla d \cdot n = 0 \tag{11}$$

where n is the outward unit normal. Use of a Biot-like equation [4] provides the normality rule:

$$G - Y_c \leq 0; \quad \dot{d} \geq 0; \quad (G - Y_c)\, \dot{d} = 0 \tag{12}$$

to which (11) applies. The above arguments show that in the present gradient-enhanced model, the damage function includes a differential term, i.e. the laplacian of damage, and that computation of the damage field requires the solution of the diffusion equation (10) with a homogeneous boundary condition.

3. NUMERICAL EXAMPLE

The damage models presented in the previous section have been numerically implemented into a customized version of the finite element code FEAP [15] along with zero-thickness cohesive elements. The structural problem that is obtained for the gradient model turns out to be convex separately with respect to the damage and displacement fields. This feature naturally suggests the use of a staggered solution scheme in which equilibrium and damage evolution are computed by means of alternate minimizations with respect to displacements and damage fields.

The setup of the discretized equations in terms of nodal displacements and damage relies upon standard arguments [21]. In particular, denoting by $\boldsymbol{\sigma}$ the Cauchy stress and $\boldsymbol{f}$ the load vector, the weak form of equilibrium for given damage field reads:

$$\int_\Omega \sigma \nabla \delta u\, \mathrm{d}x + \int_\Gamma t \delta s\, \mathrm{d}x - f \delta u = 0 \quad \forall \delta u \tag{13}$$

The above equations require no special treatment to be solved since the admissible displacement variations $\boldsymbol{\delta u}$ are elements of a linear space. On the contrary, for fixed displacements, damage evolution is governed by a variational inequality:

$$\int_\Gamma (\boldsymbol{c \nabla d\, \delta \nabla d} - (\boldsymbol{Y - Y_c})\boldsymbol{\delta d})\, \mathbf{d}\boldsymbol{x} \leq \mathbf{0} \tag{14}$$

with admissible variations $\boldsymbol{\delta d}$ such that $\boldsymbol{\delta \dot{d}} \geq \mathbf{0}$. In the numerical application documented hereafter, the bulk material is discretized using a structured mesh made of quadrilateral elements with enhanced strains whereas for the interface use is made of zero-thickness elements that have been specifically designed for the treatment of the problem at hand. All computations have been carried out using an arc-length algorithm and a termination criterion expressed in terms of the incremental energy norm as:

$$E^i \leq \rho E^0 \tag{15}$$

with a tight tolerance $\rho = 10^{-16}$.

3.1. Mode-I Test Problem

We consider a Double Cantilever Beam (DCB) structure (Fig. 3) with dimensions close to the ones adopted in experiments for measuring the mode-I fracture energy, see also [17]. The adherends consists of two equal arms of thickness h = 8 mm, length L = 200 mm and width b = 20 mm made of Al 2024-T351; the elastic properties are E = 73 GPa, ν = 0.33 with initial flaw a = 50 mm. The material properties for the interface are taken as G_c = 0.5 N/mm, Y_0 = 0.05 N/mm, k^+ = 8000 N/mm^3, to which corresponds a peak stress σ_c of the local cohesive law of about 40 MPa.

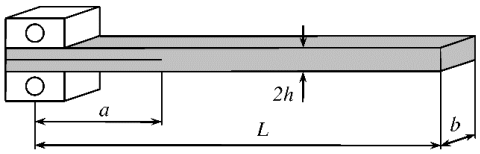

Fig. 3. Scheme of the DCB specimen

Loading is simulated by prescribing a target displacement via arc-length control; the problem is solved first with the local model and then using the gradient-based formulation.

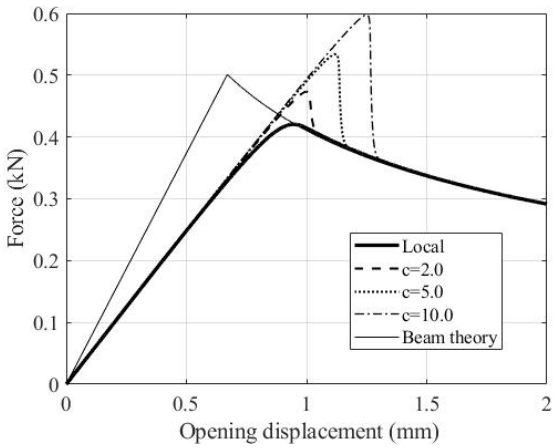

Fig. 4. DCB specimen. Computed responses

In the numerical simulation of the symmetric DCB, plane stress conditions are considered. The right-end of the structure is free while the boundary conditions on the left part consist of two supports (rotation of the specimen ends is allowed), one of which is subject to an increasing vertical displacement during the test, which in experiments is usually carried out using a universal tension-compression apparatus.

The computed load–deflection curves are depicted in figure 4 in terms of the reaction force P versus the opening displacement for the local and the nonlocal model at varying gradient parameter c. In the same figure is also shown the analytical solution obtained via Euler-Bernoulli beam theory, according to which the opening displacement at crack propagation reads:

$$\delta = \frac{\left(3EG_c^3 b^4 h^3\right)^{\frac{1}{2}}}{9P^2} \tag{16}$$

Two effects of the gradient enhancement on the structural response are apparent. The first one is the swelling of the curves obtained with the gradient model and a progressive increase of the peak load with the gradient parameter c; the second one is convergence of all the computed curves to the propagation curve of elementary beam theory, which corresponds to a steady-state condition. The same effects are clearly visible also in Figure 5, where the experimental curve labelled EP/n_EXP taken from [9] is compared with the numerical results obtained via the models presented in the previous section; the fracture energy used for computations, i.e. G_c = 1.58 N/mm, has been obtained via residual minimization as done in [17]. One can notice that the computed propagation curves do overlap with the terminal part of the experimental one; swelling of the experimental curve with respect to the one predicted using the local cohesive zone model is also evident. At this stage, such comparison has to be intended for a preliminary, empirical validation of the gradient formulation since the full calibration of the model is outside of the scope of the present work

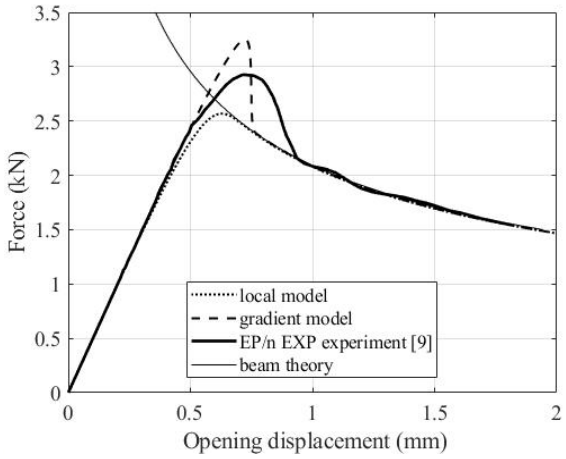

Fig. 5. Model response vs experiment of reference [9]

The effect of the gradient enhancement on the stress distributions along the interface is shown in figure 6. The diagrams refer to opening displacements ranging from 0.8 to 1.3 mm, which roughly correspond to displacement levels at which the traction profiles for given values of the gradient parameter start to develop towards the steady state. In the first diagram (δ=0.8 mm) the stress distributions for $c > 0$ are almost superposed, which reflects the fact that the relevant equilibrium curves are close to the initial loading line; contrariwise, the tractions profile of the local model has already started to move. For δ=1.0 mm the crack propagation stage has been attained for the local model only, see figure 4, and the relevant traction profile has reached a shape that will no change any longer.

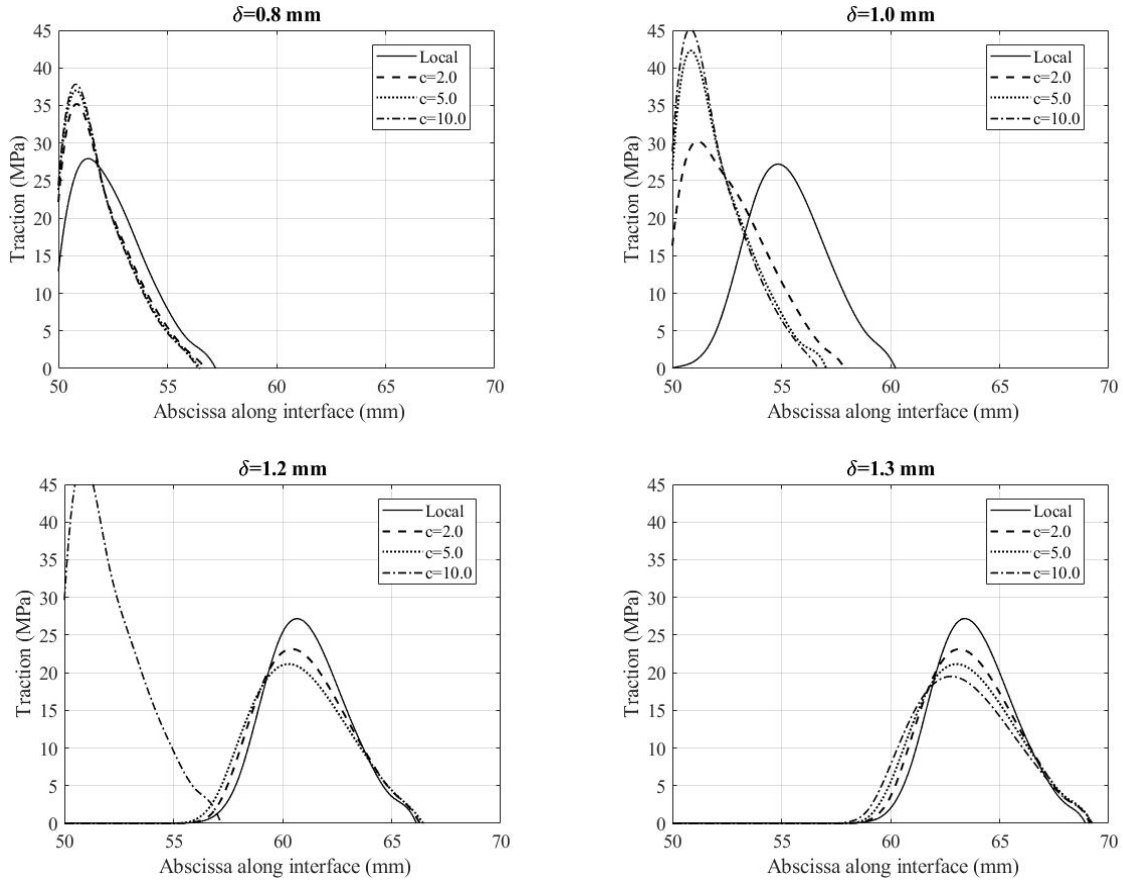

Fig. 6. DCB specimen. Tractions profiles along the interface at different stages of the loading program

The tractions of the gradient model also start to change their profile for δ=1.0 mm and will progressively reach their final form for displacement levels that increase with the gradient parameter c. Finally, the last diagram of figure 6, which refers to δ=1.3 mm, puts forward the global effect of the gradient model in terms of traction distributions, whereby the peak stresses at the steady state are lowered compared to the local model.

Figure 7 displays the damage distributions along the interface for increasing opening displacements. Besides the smoothing effect due to nonlocality, here one can notice that the damage process zone grows and reaches its maximum size at different stages of the loading process depending on the gradient activity parameter c. In particular, for the considered DCB problem, the final length of the damage zone varies between 12 mm for the local model to a maximum of 32 mm for the gradient model with c=10 N. A damage profile that is completely developed corresponds to the attainment of the steady state and from this point onwards, the process zone starts moving along the interface with no change in shape. This effect is clearly shown in the last two diagrams in figure 6 that refer to δ=1.3 mm and δ=2.0 mm, which differ only for a translation along the horizontal axis.

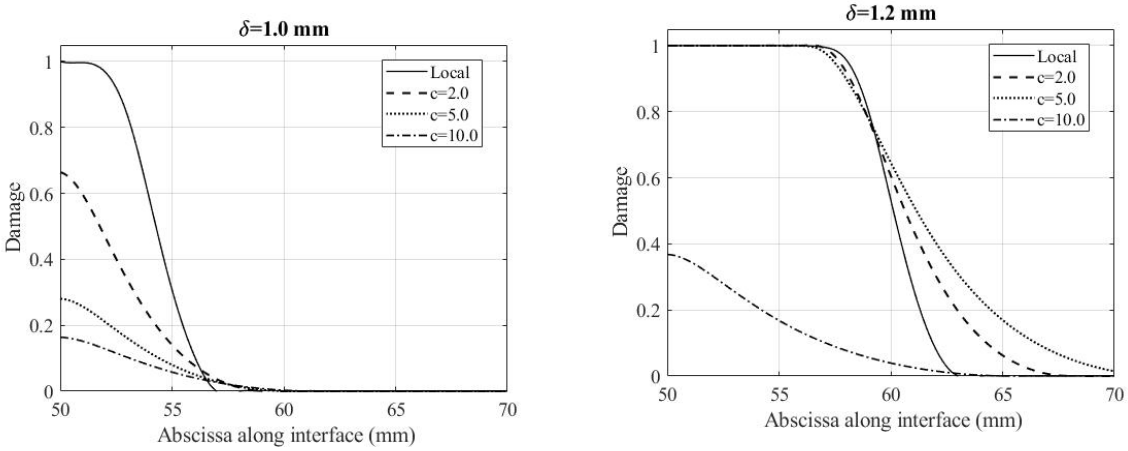

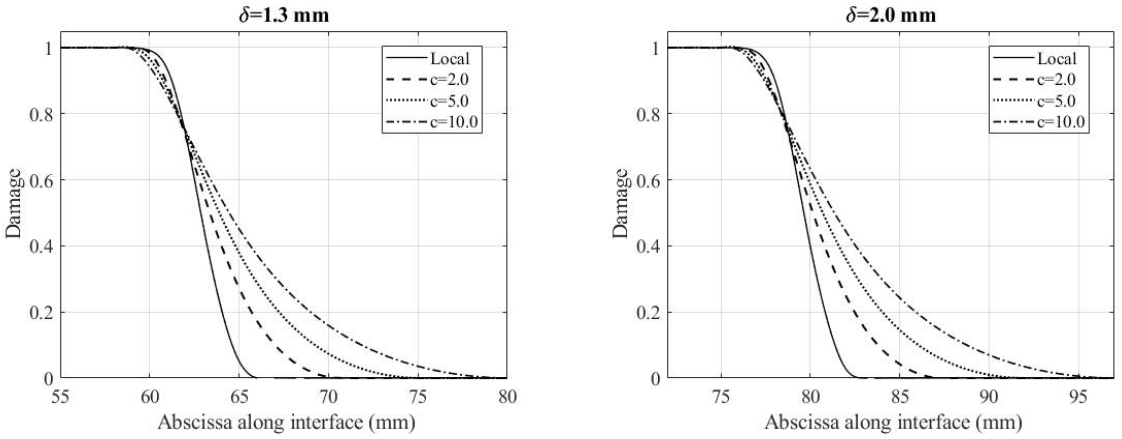

Fig. 7. DCB specimen. Damage distributions along the interface at different stages of the loading program

4. CONCLUSIONS

In the paper a new cohesive model is presented for the simulation of interfacial decohesion and fracture in adhesive joints. It is based on a gradient of damage regularization complying with the framework of generalized standard materials and leads to an isotropic diffusion equation for damage evolution that is coupled to the equilibrium equations. The model has been implemented in a multi-field finite element setting along with zero-thickness interface elements that are specifically designed to deal with the problem at hand.

The numerical results obtained for a symmetric DCB problem have revealed the main features of the gradient model. In particular, it is shown that the material parameter that plays the role of diffusion coefficient is linked to the size of the damage process zone, which expands monotonically with gradient activity. Moreover, both damage and stress profiles are smoothed across elements, thus allowing for coarse finite element meshes.

The mode-I test problem has confirmed the consistency of the method, for which extensions to mixed-mode situations and higher order elements as well as model calibration will be the object of forthcoming papers.

REFERENCES

[1] **Adams R. D.,** *Adhesive Bonding. Science, Technology, and Applications* (Second Edition), Woodhead Publishing, Duxford, United Kingdom, 2021.

[2] **Anderson T. L.,** *Fracture Mechanics Fundamentals and Applications (Fourth Edition)*, CRC Press, Boca Raton, USA, 2017.

[3] **Barenblatt G. I.,** *The mathematical theory of equilibrium cracks in brittle fracture*, Advances in Applied Mechanics, vol. 7, 1962, pp. 55-129.

[4] **Biot M. A.,** *Mechanics of Incremental Deformations*, John Wiley and Sons, New York, USA, 1965.

[5] **Halphen B., Nguyen Q.S.,** *Sur les matériaux standard généralisés*, Journal de Mécanique, vol. 14, 1975, pp.39–63.

[6] **Harper P. W., Hallett S. R.**, *Cohesive zone length in numerical simulations of composite delamination*, Engineering Fracture Mechanics, vol. 75, 2008, pp. 4774-4792.

[7] **Hillerborg A., Modéer M., Petersson P.-E.,** *Analysis of crack formation and crack growth in concrete by means of fracture mechanics and finite elements*, Cement and Concrete Research, vol. 6, 1976, pp. 773-781.

[8] **Lorentz E, Benallal A.,** *Gradient constitutive relations: numerical aspects and application to gradient damage*, Computer Methods in Applied Mechanics and Engineering, vol.194, 2005, pp. 50-52.

[9] **Khabaz-Aghdam A., Dizaji S. A., Choupani N., da Silva L. F. M.,** *Failure analysis of adhesively bonded joints using a modulatory damage model*, Engineering Failure Analysis, vol. 163, Part B, 2024, 108602.

[10] **Mi Y., Crisfield M. A., Davies G. A. O., Hellweg H. B.,** *Progressive delamination using interface elements*, Journal of Composite Materials, vol. 32, 1998, pp. 1246-1272.

[11] **Nabarro F.,** *Dislocations in a simple cubic lattice*, Proceedings of the Physical Society, vol. 59, 1947, pp. 256-272.

[12] **Peerlings R., de Borst R., Brekelmans W., De Vree J.,** *Gradient enhanced damage for quasi-brittle materials*, International Journal for Numerical Methods in Engineering, vol. 39, 1996, pp. 3391-3403.

[13] **Peerlings R., Geers M., de Borst R., Brekelmans W.,** *A critical comparison of nonlocal and gradient-enhanced softening continua*, International Journal of Solids and Structures, vol. 38, 2001, pp. 7723-7746.

[14] **Quan D., Murphy N., Ivankovic A.,** *Fracture behaviour of epoxy adhesive joints modified with core-shell rubber nanoparticles*, Engineering Fracture Mechanics, vol. 182, 2017, pp. 566-576.

[15] **Taylor R.L.,** *FEAP A Finite Element Analysis Program Programmer Manual.* University of California at Berkekey, 2022.

[16] **Valoroso N., Champaney L.,** *A damage-mechanics-based approach for modelling decohesion in adhesively bonded assemblies*, Engineering Fracture Mechanics, vol. 73, 2006, pp. 2774-2801.

[17] **Valoroso N., Sessa S., Lepore M., Cricrì G.,** *Identification of mode-I cohesive parameters for bonded interfaces based on DCB test*, Engineering Fracture Mechanics, vol. 104, 2013, pp. 56-79.

[18] **Valoroso N., de Barros S.,** *Adhesive joint computations using cohesive zones*, Applied Adhesion Science, vol. 1, 2013, pp. 1-9.

[19] **Valoroso, N., Stolz, C.,** *Progressive Damage in Quasi-brittle Solids*, In: Carcaterra, A. et al. (eds), Proceedings of XXIV AIMETA. Springer, Cham, 2020, pp. 408-418.

[20] **Valoroso N., Stolz C.,** *Graded damage in quasi-brittle solids*. International Journal for Numerical Methods in Engineering, vol. 123, 2022, pp. 2467-2498.

[21] **Zienkiewicz O. C., Taylor R. L., Fox D.,** *The Finite Element Method for Solid and Structural Mechanics (Seventh Edition)*, Butterworth-Heinemann, Oxford, United Kingdom, 2014.